Am J Transl Res 2026;18(2):1672-1689
www.ajtr.org /ISSN:1943-8141/AJTR0170688

Original Article

Radix Aconiti Lateralis Preparata and *Coptidis Rhizoma* mitigate the course of acute myeloid leukemia

Peng Hu[1,2], Jie Zhao[2], Zhi-Xiang Lu[2], Qi Wang[2], Xiao-Li Gao[2], Zheng-Zheng Li[2], Tong-Hua Yang[1,2]

[1]Faculty of Life Science and Technology, Kunming University of Science and Technology, Kunming 650500, Yunnan, P. R. China; [2]Department of Hematology, The First People's Hospital of Yunnan Province, Affiliated Hospital of Kunming University of Science and Technology, Kunming 650500, Yunnan, P. R. China

Received December 11, 2025; Accepted February 4, 2026; Epub February 15, 2026; Published February 28, 2026

Abstract: Objectives: Radix Aconiti Lateralis Preparata (RALP) and Coptidis Rhizoma (CR) demonstrated efficacy in mitigating malignant phenotypes across various tumors types. Therefore, this research aimed to assess the impact of RALP and CR on tumor burden in acute myelocytic leukemia (AML). Methods: *In vitro*, AML cell lines were treated with a range of RALP and CR concentrations over varying durations to determine the optimal inhibitory concentrations. *In vivo*, an AML model was established in NSG mince using Luc-MOLM-13 cells. The effects of RALP and CR on AML tumor burden were subsequently evaluated via *in vivo* imaging and histopathological analysis. Potential therapeutic targets of RALP and CR in AML were identified using network. Results: Monotherapy with either RALP or CR effectively reduced AML cell viability, with maximal inhibition observed at 100 μg/ml for 72 hours. *In vitro*, both agents attenuated AML cell proliferation and increased apoptosis, with the combination treatment exhibiting a synergistic effect. *In vivo*, RALP and/or CR treatment alleviated model-associated weight loss, reduced Luc-MOLM-13 cell infiltration, and decreased bone marrow $hCD45^+$ cells, with the combination regimen proving most effective. Network pharmacology identified 9 and 57 potential AML-related targets for RALP and CR, respectively. These targets regulate apoptosis, inflammation, proliferation, and immunity. Notably, hub proteins among these targets were effectively regulated by RALP and/or CR treatment, including CALM1, CASP3, CHEK1, ESR1, IL-6, MYC, and PTGS2. Conclusions: As traditional Chinese medicine, RALP and CR effectively alleviate AML tumor burden, and their combination demonstrates synergistic effects.

Keywords: Acute myeloid leukemia, traditional Chinese medicine, Radix Aconiti Lateralis Preparata, *Coptidis Rhizoma*, network pharmacology

Introduction

Acute myeloid leukemia (AML) is an aggressive hematologic malignancy characterized by the abnormal differentiation and clonal proliferation of myeloid progenitor cells, representing the most clinically challenging form of leukemia [1]. Globally, leukemia accounts for approximately 474,519 new cases annually, constituting 2.5% of total cancer incidence, and results in roughly 35,000 deaths, representing 3.1% of cancer-related mortality, particularly in Australia-New Zealand [2]. The standard treatment paradigm for AML involves initial induction chemotherapy to achieve complete remission, typically followed by consolidation and/or maintenance therapy. The traditional "7+3" cytarabine and anthracycline regimen remains a cornerstone of initial treatment [3, 4]. However, while many patients attain remission, chemotherapy is associated with significant toxicity, and a substantial proportion experience relapse or develop refractory disease, leading to poor long-term outcomes [5]. Consequently, the overall five-year survival rate for AML patients remains below 30% [3]. There is therefore a pressing need to elucidate the underlying pathogenesis of AML and to develop more effective and tolerable therapeutic strategies to improve patient survival.

Traditional Chinese medicine (TCM) is recognized for its potential to alleviate the progression of AML, owing to its low side effects, limited toxicity, multi-component, and multi-target nature, including arsenic, curcumin, quercetin,

https://doi.org/10.62347/UXGV2334

and ginsenosides [6]. Notably, omacetaxine, a semi-synthetic derivative of homoharringtonine obtained from *Cephalotaxus harringtonia* var. *drupacea*, has received Food and Drug Administration approval for leukemia treatment. Furthermore, multiple studies indicate that integrating TCM with western medicine (WM) can yield superior therapeutic outcomes compared to WM alone for various diseases [7-9]. Fuzi, or Radix Aconiti Lateralis Preparata (RALP), is prepared from the tuberous roots of *Aconitum carmichaeli Debx*. Its primary bioactive constituents include aconitine alkaloids, flavonoids, polysaccharides, sterols, and organic acids [10]. Huanglian, or *Coptidis Rhizoma* (CR), is a perennial herb belonging to the Ranunculaceae family. Its key active compounds are berberine, isoquinoline alkaloids, lignans, and flavonoids [11]. Preclinical studies at the cellular and animal levels have demonstrated that RALP and CR can alleviate tumor burden in various cancers, including non-small cell lung cancer [12, 13], liver cancer [14, 15], colorectal cancer [16, 17], breast cancer [17, 18], and gastric cancer [17]. Nevertheless, the therapeutic potential of RALP and CR specifically for AML remains to be elucidated.

This study investigated the anticancer effects of RALP and CR using AML-related cells and NSG mouse models. Potential molecular targets were identified through network pharmacology. We demonstrate that RALP and CR alleviate the AML tumor burden *in vivo* and *in vitro*, with evidence of a synergistic interaction. Notably, CALM1, CASP3, CHEK1, ESR1, IL-6, MYC, and PTGS2 were identified as potential therapeutic targets of RALP and CR. Collectively, these findings provide an experimental foundation and suggest molecular mechanisms supporting RALP and CR as potential adjunct therapies for AML.

Materials and methods

Network pharmacology analysis

Active ingredients of RALP and CR, along with known AML-related targets, were identified using the TCMSP [19] and DisGeNET [20] databases. Active ingredients were screened based on the following thresholds: drug-likeness (DL) >0.18 and oral bioavailability (OB) >30%. Overlapping targets for RALP and CR in AML treatment were identified using jvenn. Protein-protein interaction (PPI) networks for these targets were constructed and visualized with CytoScape software (NHGRI, USA). Hub proteins within the overlapping target sets were analyzed using the STRING database [21] and CytoScape software. Gene Ontology (GO) and Kyoto Encyclopedia of Genes and Genomes (KEGG) enrichment analyses were performed using the clusterProfile package [22] in R software, with results visualized using the ggplot2, igraph, and ggraph packages [23].

Culture and treatment of AML cells

The human AML cell lines MOLM-13 and HL-60, authenticated by short tandem repeat profiling, were purchased from the respective vendors: BLUEFBIO (Shanghai) Biotechnology Development Co., Ltd. (Cat No. BFN60804425) and Procell (Wuhan) Life Science and Technology Co., Ltd. (Cat No. CL-0110). Cells were inoculated in high-glucose dulbecco's modified eagle medium (DMEM) (Cat No. G4515, Servicebio, China) supplemented with fetal bovine serum (10%; Cat No. 10099-141, Gibco, China) and penicillin-streptomycin (1%; Cat No. 1902417, Gibco, China).

RALP and CR were purchased from the Yunnan Provincial Hospital of Traditional Chinese Medicine. For each extract, 200 ml of double-distilled water was added, followed by two cycles of reflux extraction (30 min each). The filtered decoction was then concentrated by rotary evaporation at 30°C to a final volume of 35 ml (equivalent to a concentration of 2 g/ml). To determine the optimal treatment concentration, cells were exposed to a range of RALP or CR concentrations (0, 1, 2, 5, 10, 20, 40, 80, 100, and 200 μg/ml) for different times (24, 48, and 72 h). Cells were randomized into the CON, CR, RALP, and CR + RALP groups. Groups were treated for 72 h as follows: the CR group with 100 μg/ml CR, the RALP group with 100 μg/ml RALP, and the combination (CR + RALP) group with 50 μg/ml of each agent.

Proliferation and apoptosis assay of AML cells

AML Cell proliferation and apoptosis were performed by a Cell Counting Kit (CCK-8; Cat No. PF00004, Proteintech, USA) and an Annexin V-fluorescein isothiocyanate (FITC)/propidium iodide (PI) Apoptosis Kit (Cat No. P-CA-201, Procell, China), respectively. For the prolifera-

Table 1. Primer sequences for RT-qPCR assay

Target	Forward	Reverse	Length (bp)
GAPDH	TTGCCCTCAACGACCACTTT	TGGTCCAGGGGTCTTACTCC	120
ESR1	CTTCAGGCTACCATTATG	TAGTCGTTATGTCCTTGA	82
PTGS2	ATTATGAGTTATGTGTTGAC	TAGGAGAGGTTAGAGAAG	107
CHEK1	ATTCTTCCATCAACTCAT	CGCTCACGATTATTATAC	159
CALM1	GGATGCTGATGGTAATGG	TTCTTCTTCACTATCTGTATCTT	88
HIF1A	CCGAGGAAGAACTATGAA	GTTGGTTACTGTTGGTATC	92
MYC	GAACAAGAAGATGAGGAAGAA	CAGAAGGTGATCCAGACT	88
CASP3	TGACATCTCGGTCTGGTA	AACATCACGCATCAATTCC	128
IL-6	GGATTCAATGAGGAGACTT	ATCTGTTCTGGAGGTACT	85

tion assay, cells were seeded into 96-well plates, with a blank control (medium only) included for each experimental group. After adding 10 μl of CCK-8 solution to each well, plates were incubated for 2 h, and the optical density at 450 nm was measured using a microplate reader (EL800; BIO-TEK, USA). For the apoptosis assay, harvested cells were washed with PBS, centrifuged at 300×g for 5 min, and resuspended in 1 × binding buffer. Cells were then stained with 5 μl of Annexin V-FITC solution and 5 μl of PI solution (50 μg/mL) and incubated for 20 min. The proportion of apoptotic cells was quantified by a flow cytometer (NovoCyte Advanteon Dx; Agilent, USA).

RT-qPCR and Western blot assay

Total RNA and protein were extracted from cells and tissues using TRIzol kit (Cat No. 15596026, Life Technologies, USA) and RIPA lysate (Cat No. PR20035, Proteintech, USA), respectively. Their concentrations were quantified with a full-wavelength microplate reader (Multiskan SkyHigh; Thermo Scientific, USA). RNA was reverse-transcribed using the FastKing RT Kit (Cat No. KR116, Tiangen, USA). qPCR was then performed with the Taq Pro Universal SYBR qPCR Master Mix (Cat No. Q712-02, Vazyme, China) on a fluorescence ration PCR instrument (7500; ABI, USA). GAPDH served as the endogenous control. Relative gene levels of target genes were calculated using the 2 (-Delta Delta C(T)). All primer sequences are listed in **Table 1**. Protein samples were separated by SDS-PAGE (Cat No. 3250GR500, BIOFFROXX, Germany) and subsequently transferred to polyvinylidene fluoride (PVDF) membranes (Cat No. FFP39, Beyotime, China). PVDF membranes were incubated with following primary and secondary antibodies: anti-GAPDH (Cat No. AF1186, Beyotime, China; 1:5,000), anti-ESR1 (Cat No. ab108398, Abcam, USA; 1:10,000), CHEK1 (Cat No. ab32531, Abcam, USA; 1:1,000), CALM1 (Cat No. ab45689, Abcam, USA; 1:10,000), MYC (Cat No. ab289980, Abcam, USA; 1:5,000), goat anti mouse IgG-HRP (Cat No. M21001L, Abmart, China; 1:4,000), and anti-rabbit IgG-HRP-linked antibody (Cat No. 7074F, CST, USA; 1:3000). Protein bands were visualized using the BeyoECL Plus Kit (Cat No. P0018S, Beyotime, China) and imaged with a gel imaging system (5200 Multi; Tanon, China).

In vivo assay

Thirty-eight SPF-grade NSG mice (NOD.Cg-*Prkdc*^{scid}*Il2rg*^{em1Smoc}), aged 6-8 weeks, were purchased from Shanghai MODEL ORGANISMS (Cat No. NM-NSG-001). A schematic of the experimental timeline, including drug administration, is provided in **Figure 8A**. All NSG mice were randomly allocated to either a NSG (n=3) or an AML (n=35) group. NSG-related AML models were established in the AML group as previously described [24, 25]. Briefly, MOLM-13 cells were transduced with a CMV-Luciferase-Puro lentivirus (Cat No. GM-02201V210, Genomeditech, China) and selected with puromycin to generate stably expressing Luc-MOLM-13 cells. Mice in the AML group received 2 × 10^5 Luc-MOLM-13 cells via tail vein injection, whereas mice in the NSG group received an equal volume of saline. On day 7 post-injection, successful engraftment was confirmed by quantifying the proportion of human CD45$^+$ (hCD45$^+$) cells in the bone mar-

row of mice from both groups (n=3 per group) via flow cytometry. Subsequently, AML model mice were randomly assigned to three treatment subgroups (n=8 each): CR, RALP, and CR + RALP. Beginning on day 8 (designated D0 for treatment), mice received oral gavage three times per week for two weeks (until D14) with the following: the CR group received 500 μg/ml CR, the RALP group received 500 μg/ml RALP, and the CR + RALP group received a combination of 500 μg/ml CR and 500 μg/ml RALP. Mice in the AML group were given an equal volume of distilled water (0.1 ml/10 g) by gavage. Tumor burden was monitored via bioluminescence imaging on days 0, 4, 7 and 14 of treatment. NSG mice were injected intraperitoneally with 15 mg/ml D-Luciferin sodium (0.1 ml/10 g; Cat No. 40901ES03, Yeasen, China) and imaged using a small animal *in vivo* imaging system (IVIS Lumina III; PerkinElmer, USA). No mice died throughout the entire animal experiment. NSG mice were euthanized on day 23 by odium pentobarbital overdose (200 mg/kg). Femur, lung, liver, and spleen samples of NSG, AML, CR, RALP, and CR + RALP groups were collected for further analysis. All animal experiments were approved by the Ethics Committee of the Affiliated Hospital of Kunming University of Science and Technology (Protocol #20220214-137).

Analysis of hCD45$^+$ cell proportion

The proportion of hCD45$^+$ cells in bone marrow and tissue sections (lung, liver and spleen) of NSG mice was assessed by flow cytometry and immunohistochemical (IHC) staining. For flow cytometry, bone marrow cells from were flushed femurs with PBS, pelleted by centrifugation (1,000×g for 3 min), and collected. Red blood cells were lysed using ACK Lysis Buffer (Cat No. C3702, Beyotime, China). Cells were then stained with 5 μl of anti-hCD45-FITC mAb (Cat No. 11-0459-42, Invitrogen, USA). An unstained sample served as a control. After a 15-min incubation, samples were analyzed on a flow cytometer (NovoCyte Advanteon Dx; Agilent, USA) with appropriate FITC excitation/emission settings (498/517 nm). For IHC staining, tissue sections of lung, liver and spleen were incubated overnight at 4°C with anti-hCD45 mAb (Cat No. 14-0459-82, Invitrogen, USA). The following day, sections were incubated with a mouse/rabbit enhanced polymer method assay system (Cat No. PV-9000, ZSGB-BIO, China). Signal was developed using a DAB kit (Cat No. ZL1-9019, ZSGB-BIO, China), counterstained with hematoxylin solution (Cat No. H3136, Sigma, USA), and mounted with neutral resin (Cat No. WG10004160, Servicebio, China). Stained sections were visualized and images were acquired using an orthogonal fluorescence microscope (BX53; Olympus, Japan).

Statistical analysis

All experiments were performed with at least three independent replicates. Data are presented as mean ± standard deviation. The Shapiro-Wilk test was used to determine the normality of the data. Comparisons between two groups were accomplished using a two-tailed student's t-test. For comparisons among three or more groups, one-way ANOVA and Tukey's multiple comparisons test or Kruskal-Wallis test and Dunn's multiple comparisons test was applied, as appropriate based on data distribution. For multi-factor comparisons, two-way ANOVA and Tukey's multiple comparisons test was applied. All statistical analyses were conducted using GraphPad Prism software. $P<0.05$ was considered statistically significant.

Results

Identification of active ingredients and targets for RALP and CR

Active ingredients of RALP and CR were identified by querying the TCMSP database using the keywords "Radix Aconiti Lateralis Preparata" and "Coptidis Rhizoma". Screening with thresholds of OB >30% and DL >0.18 yielded 21 active ingredients for RALP and 14 for CR (Supplementary File 1). The compounds with the highest OB in RALP and CR were ignavine and corchoroside A_qt, respectively, while those with the highest DL were neokadsuranic acid B and worenine, respectively. The ingredients were associated with 20 and 84 predicted targets for RALP and CR, respectively (Supplementary File 2). To identify potential therapeutic targets for AML, genes associated with AML were retrieved from the DisGeNET database and intersected with the predicted targets of RALP and CR. The DisGeNET database contained 3,111 AML-related genes

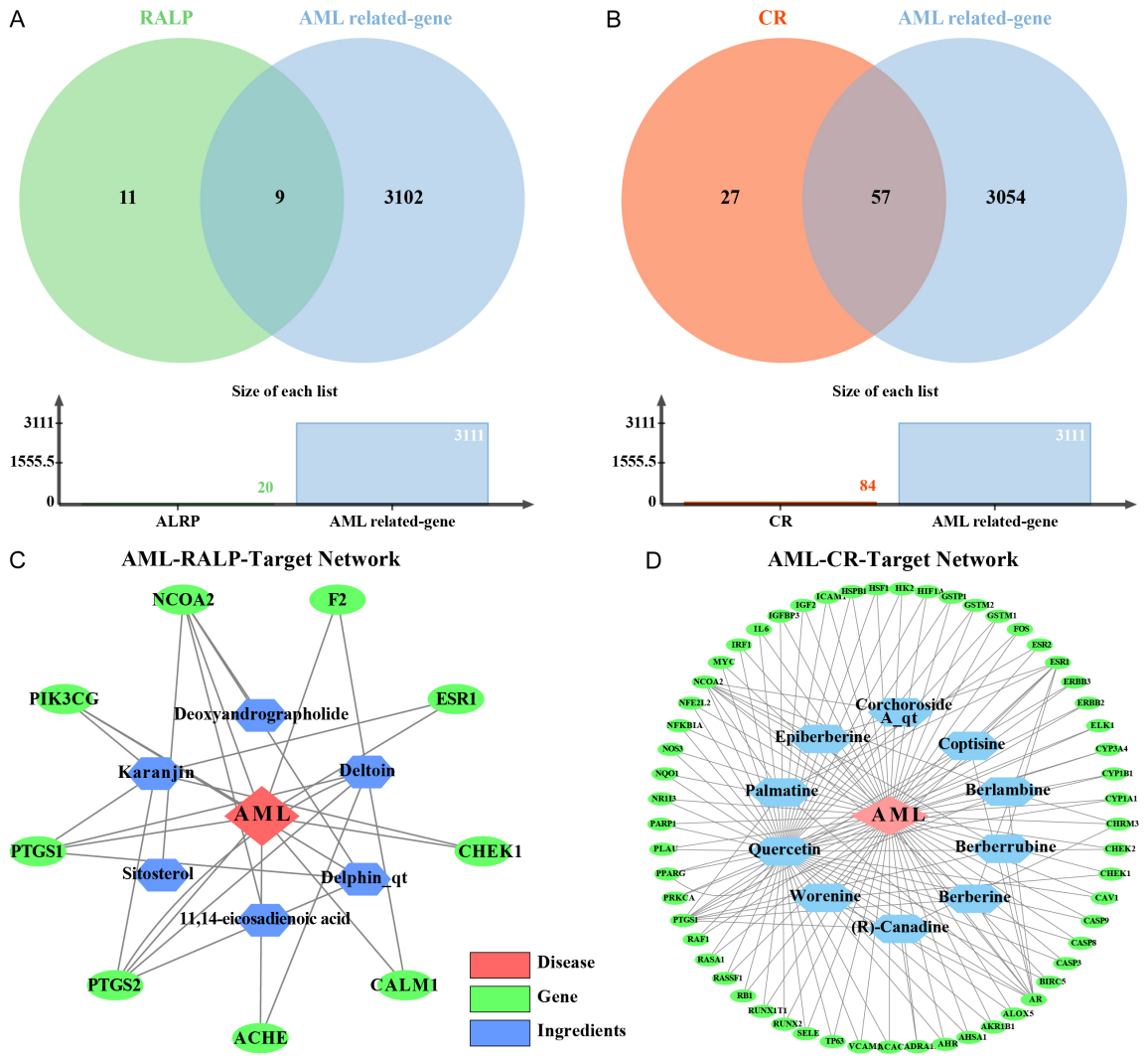

Figure 1. Network pharmacology analysis identifies active ingredients and putative targets of Radix Aconiti Lateralis Preparata (RALP) and Coptidis Rhizoma (CR) in acute myelocytic leukemia (AML). (A, B) Venn diagrams showing the overlap between predicted targets of RALP (A) or CR (B) and known AML-associated genes. Active ingredients were filtered by drug-likeness (DL) >0.18 and oral bioavailability (OB) >30%. Green, orange, and blue represent the effective component targets of RALP, effective component targets of CR, and AML-related genes, respectively. (C, D) AML-RALP-Target (C) and AML-CR-Target networks (D) were visualized using CytoScape software. Red, green, and blue represent diseases, genes, and effective components, respectively.

(Supplementary File 3). Venn diagrams revealed that 9 and 57 overlapping targets between the RALP and CR target sets and the AML gene set respectively (**Figure 1A**, **1B**). The AML-RALP-Target network comprised 6 active ingredients and 9 overlapping targets. Within this network, NCOA2 was connected to the most ingredients (sitosterol, 11,14-eicosadienoic acid, deoxyandrographolide, and Delphin_qt) (**Figure 1C**). The AML-CR-Target network contained 10 active ingredients and 57 overlapping targets, with PTGS1 being the target linked to the most compounds, including palmatine, palmatine, worenine, (R)-canadine, berberine, berberrubine, berlambine, and coptisine (**Figure 1D**). These findings suggest that the anti-AML effects of RALP and CR may be mediated through these overlapping targets.

Identification of hub gene and enrichment analysis for the overlapping targets of RALP and CR

To identify hub proteins within the overlapping targets, PPI networks were constructed. As shown in **Figure 2A**, the RALP-specific network

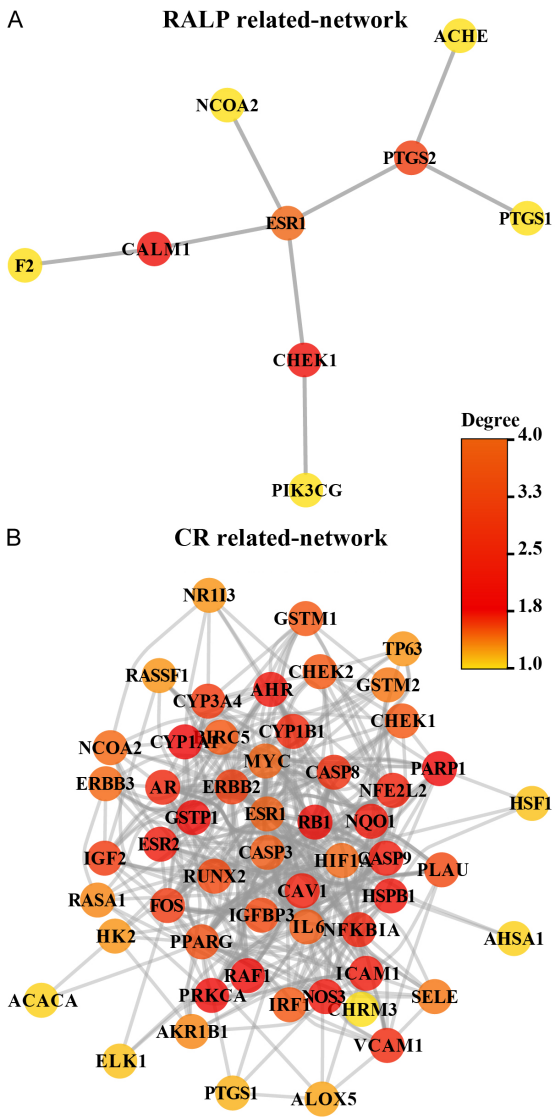

ID	Degree	Betweenness Centrality	Closeness Centrality
ESR1	4	0.82142857	0.66666667
PTGS2	3	0.46428571	0.53333333
CALM1	2	0.25	0.47058824
CHEK1	2	0.25	0.47058824
ACHE	1	0	0.36363636
F2	1	0	0.33333333
PIK3CG	1	0	0.33333333
NCOA2	1	0	0.42105263
PTGS1	1	0	0.36363636

ID	Degree	Betweenness Centrality	Closeness Centrality
HIF1A	38	0.10510594	0.77142857
MYC	37	0.07885195	0.76056338
ESR1	36	0.06548693	0.73972603
IL6	35	0.10376734	0.73972603
CASP3	35	0.06282555	0.73972603
PPARG	32	0.09383346	0.71052632
ERBB2	28	0.03227513	0.66666667
FOS	27	0.03328136	0.66666667
CASP8	24	0.01802308	0.64285714
AR	22	0.01555074	0.62068966

Figure 2. Protein-protein interaction (PPI) network of overlapping targets. (A, B) The PPI network of the overlapping targets of RALP (A) and CR (B) predicted and visualized using the STRING database and CytoScape software. A deeper red color indicates a higher degree. The table shows the top ten proteins ranked by degree, along with their corresponding betweenness centrality and closeness centrality. RALP, Radix Aconiti Lateralis Preparata; CR, Coptidis Rhizoma.

comprised 9 nodes and 8 interaction pairs, with ESR1, PTGS2, CALM1, and CHEK1 displaying the highest degree centrality. The CR-specific network, consisting of 55 nodes and 413 interaction pairs, identified HIF1A, MYC, ESR1, IL6, CASP3, and PPARG as top-ranked hub proteins based on degree (**Figure 2B**). These proteins represent potential key targets through which RALP and CR may regulate AML progression.

GO and KEGG pathway enrichment analyses were performed to elucidate the biological functions and mechanisms associated with the overlapping targets. GO analysis for the 9 RALP-overlapping targets revealed significant enrichment in biological processes including metal ion transport, inflammatory response, prostaglandin synthesis, myeloid leukemia-mediated immunity, oxidative stress, and lipid metabolism (**Figure 3A**). A clustered representation of these enriched GO terms is provided in **Figure 3B**. Specifically, PTGS2 and F2 were associated with metal ion transport, inflammatory responses, and prostaglandin synthesis (**Figure 3C**). For the 57 CR-overlapping targets,

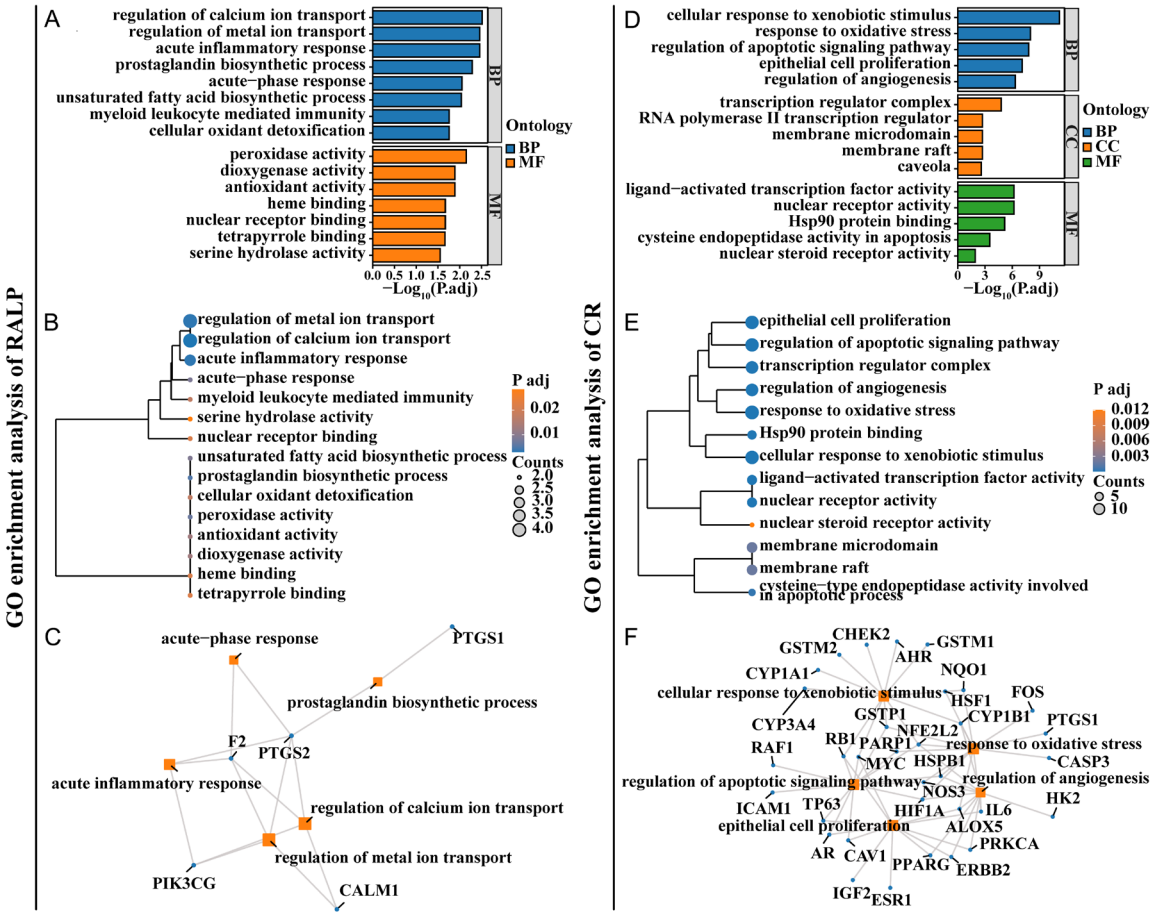

Figure 3. Gene Ontology (GO) enrichment analysis of overlapping targets. (A, D) Bar charts of the top 15 GO significantly enriched GO terms, ranked by -$\log_{10}$ *P*.adj for overlapping targets of RALP-AML (A) and CR-AML (D). Orange, blue, and green represent CC (cellular component), BP (biological process), and MF (molecular function), respectively. (B, E) The clustering tree displays the relationships among the top 15 GO terms ranked by -$\log_{10}$ *P*.adj for the overlapping targets of RALP (B) and CR (E). (C, F) The network diagram visualizes the relationships between the overlapping targets of RALP (C) and CR (F) and the GO terms. The circles and squares represent the overlapping targets and GO terms, respectively. RALP, Radix Aconiti Lateralis Preparata; CR, Coptidis Rhizoma; AML, acute myelocytic leukemia.

analysis identified predominant roles as transcriptional regulators, with enrichment in processes such as extracellular stimulus responses, oxidative stress, apoptosis, proliferation, angiogenesis, and transcriptional regulation (**Figure 3D**, **3E**). As revealed in **Figure 3F**, HIF1A, MYC and ESR1 were implicated in oxidative stress, apoptosis, extracellular stimulus response and proliferation. KEGG enrichment analysis for RALP targets indicated enrichment in signaling pathways such as oxytocin, estrogen, cGMP-PKG, phospholipase D, Apelin and C-type lectin receptor signaling pathways (**Figure 4A**, **4B**). Moreover, PTGS2 was associated with arachidonic acid metabolism, lipid metabolism and oxytocin signaling pathway (**Figure 4C**). For CR targets, enriched KEGG pathways included MAPK, TNF, p53, VEGF, AGE-RAGE and thyroid hormone (**Figure 4D**, **4E**). HIF1A, MYC and ESR1 were associated with pathways related to platinum drug resistance, chemical carcinogenesis-receptor activation, lipid and atherosclerosis, hepatocellular carcinoma and proteoglycans in cancer (**Figure 4F**). These enrichment analyses suggest that the overlapping targets of RALP and CR may influence AML process by modulating oxidative stress, apoptosis, drug resistance, inflammatory response, proliferation, immune response and angiogenesis.

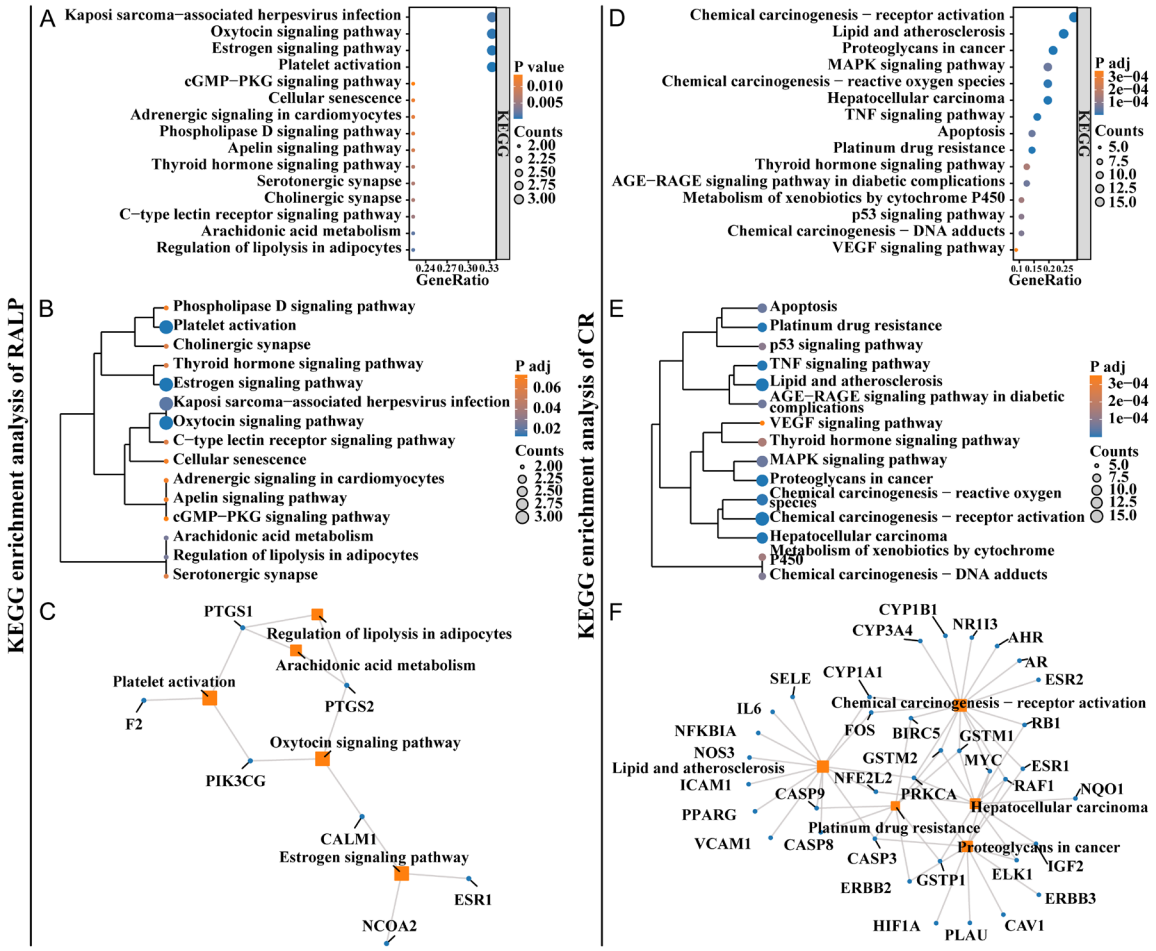

Figure 4. Kyoto Encyclopedia of Genes and Genomes (KEGG) enrichment analysis for the overlapping targets of RALP and CR. (A, D) The bar charts display the top 15 KEGG pathways ranked by -$\log_{10}$ *P*.adj from the KEGG enrichment analysis of the overlapping targets of RALP (A) and CR (D). (B, E) The clustering tree displays the relationships among the top 15 KEGG pathways ranked by -$\log_{10}$ *P*.adj for the overlapping targets of RALP (B) and CR (E). The color and size of the points represent the statistical results and the number of overlapping targets, respectively. (C, F) The network diagram visualizes the relationships between the overlapping targets of RALP (C) and CR (F) and the KEGG pathways. The circles and squares represent the overlapping targets and KEGG pathways, respectively. RALP, Radix Aconiti Lateralis Preparata; CR, Coptidis Rhizoma; AML, acute myelocytic leukemia.

RALP and/or CR alleviate the growth of MOLM-12 and HL-60 cells in vitro

Based on the identified overlap between RALP/CR targets and AML-related genes, we hypothesized that RALP and CR possess therapeutic potential against AML. We first investigated the effects of RALP and CR, individually and in combination, on AML cell proliferation and apoptosis *in vitro*. Two-way ANOVA analysis revealed significant differences in cell viability when MOLM-12 and HL-60 cells were treated with different concentrations of RALP and CR for different durations (**Figure 5A**, **5B**). As demonstrated in **Figure 5A**, CR treatment reduced the viability of MOLM-13 and HL-60 cells in a concentration-dependent manner. Statistically significant reductions in MOLM-13 cell viability were observed at 200 μg/ml CR after 24 h and 48 h, and at 10 μg/ml after 72 h. The IC_{50}-24 h, IC_{50}-48 h and IC_{50}-72 h of CR in MOLM-13 cells were 618.9 μg/ml, 607.0 μg/ml and 452.5 μg/ml respectively. For HL-60 cells, significant effects occurred at 80 μg/ml CR across all time points. The IC_{50}-24 h, IC_{50}-48 h and IC_{50}-72 h of CR in HL-60 cells were 603.0 μg/ml, 396.8 μg/ml and 356.0 μg/ml respectively. Similarly, RALP inhibited the viability of both cell lines in a dose-dependent manner (**Figure 5B**). Overall, both TCMs were more potent against HL-60 cells than against MOLM-13 cells, and CR exhibited greater effi-

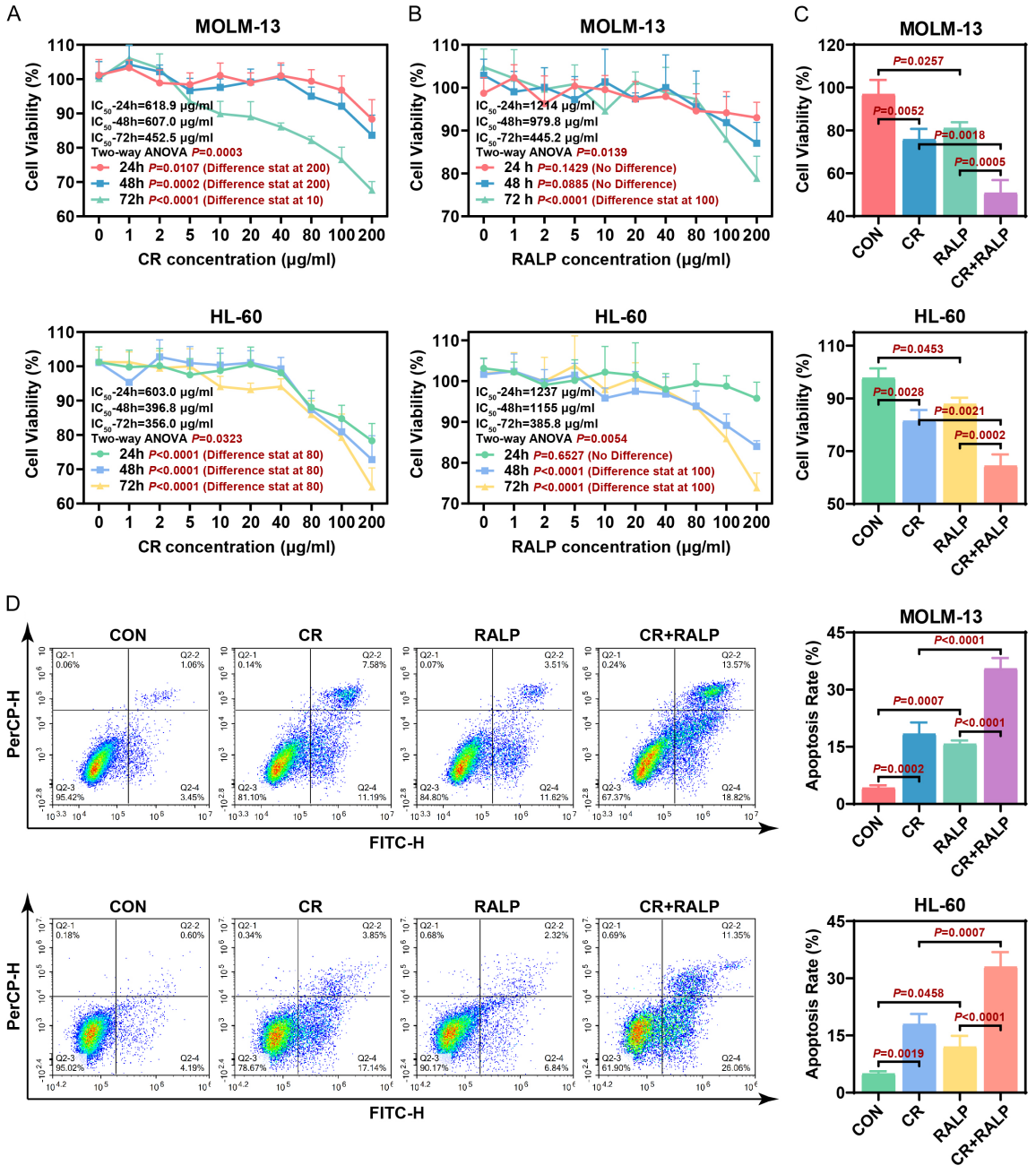

Figure 5. RALP and/or CR alleviate the growth of MOLM-12 and HL-60 Cells *in vitro*. (A, B) After treatment with different concentrations (0, 1, 2, 5, 10, 20, 40, 80, 100, and 200 μg/ml) of RALP (A) and CR (B) for various durations (24, 48, and 72 h), the Cell Counting Kit-8 (CCK-8) assay was used to assess the viability of MOLM-12 and HL-60 cells (n=3). (C) After 72 hours of treatment with 100 μg/ml RALP and/or CR, the differences in viability among the groups of MOLM-12 and HL-60 cells were analyzed. The upper and lower figures represent MOLM-12 and HL-60 cells, respectively (n=3). (D) The Annexin V-fluorescein isothiocyanate (FITC)/propidium iodide (PI) Kit combined with flow cytometry analyzed the differences in the apoptosis rates of MOLM-12 and HL-60 cells among the Con, CR, RALP, and CR + RALP groups (n=3). RALP, Radix Aconiti Lateralis Preparata; CR, Coptidis Rhizoma; AML, acute myelocytic leukemia.

cacy than RALP. Based on these dose- and time-response profiles, a concentration of 100 μg/ml for each TCM and a 72-hour treatment duration were selected for subsequent combi-

nation experiments. Treatment with 100 μg/ml of either agent alone significantly reduced cell viability, and the combination of CR and RALP demonstrated a synergistic effect (**Figure 5C**). Additionally, both CR and RALP monotherapies effectively increased apoptosis of MOLM-12 and HL-60 cells, and the combination treatment resulted in a further significant increase in apoptotic cells (**Figure 5D**). These data demonstrate that CR and RALP are effective at mitigating AML cell growth and exhibit synergistic activity *in vitro*.

RALP and/or CR modulate target expression in MOLM-12 and HL-60 cells

We next sought to experimentally validate whether RALP and/or CR modulate the expression of the predicted overlapping targets (CALM1, CASP3, CHEK1, ESR1, HIF1A, IL-6, MYC, and PTGS2) in AML cells. In MOLM-13 cells, CR and RALP monotherapy effectively downregulated the mRNA levels of *CALM1*, *CHEK1* and *IL-6*, and had no significant effect on *HIF1A* (**Figure 6A**). The effects of CR on *ESR1* and *MYC* mRNA levels and of RALP on *CASP3* and *PTGS2* mRNA levels were specific. Moreover, the combined treatment had a synergistic effect on the mRNA levels of *IL-6*, *CASP3*, *ESR1* and *MYC*. In HL-60 cells, monotherapy effectively downregulated *CALM1*, *CHEK1*, *IL-6* and *PTGS2*, upregulated *ESR1*, and had no significant effect on *HIF1A* (**Figure 6B**). The effects of CR on *MYC* and RALP on *CASP* were specific. Moreover, the combined treatment had a synergistic effect on the influence of *CHEK1*, *CASP3* and *ESR1*.

Based on the results of RT-qPCR, we selected overlapping targets CALM1, CHEK1, ESR1, and MYC for western blotting validation. In MOLM-13 cells, both CR and RALP monotherapy effectively downregulated CALM1 protein level (**Figure 7A**). The effects of CR on the protein levels of ESR1 and MYC and of RALP on the protein level of CHEK1 were specific. Moreover, the combined treatment had a synergistic effect on the influence of ESR1 and MYC proteins. In HL-60 cells, monotherapy effectively downregulated CHEK and upregulated ESR1 (**Figure 7B**). The effects of CR on MYC and RALP on CALM1 were specific. Moreover, the combination treatment had a synergistic effect on the effects of CHEK1 and ESR1.

RALP and/or CR mitigate the burden of AML in vivo

The experimental timeline, including drug administration schedules, is illustrated in **Figure 8A**. Successful engraftment was confirmed on day 7, as evidenced by a significant increase in the proportion of $hCD45^+$ cells in the bone marrow of the AML group compared to control group (**Figure 8B**). This result indicates that the success rate of AML model construction is 100%. Two-way ANOVA analysis revealed that CR and RALP treatments had significant effects on the fluorescence of Luc-MOLM-13 cells and body weight in the AML model (**Figure 8C**, **8D**). The fluorescence of Luc-MOLM-13 cells in the AML model was markedly reduced from D4 onward of CR and RALP treatment. Furthermore, the combination of CR and RALP exhibited a synergistic effect from day 7 onward (**Figure 8C**). Notably, on day 23, treatment with CR or RALP alone effectively increased mouse weight, and the combination treatment showed a synergistic effect (**Figure 8D**). On day 23, all treatment regimens effectively alleviated the Luc-MOLM-13-induced increase in the proportion of $hCD45^+$ cells in the bone marrow (**Figure 8E**). The combination therapy was more effective than either monotherapy. Pathological staining revealed extensive tumor and immune cell infiltration, along with a pronounced increase in $hCD45^+$ cells in the AML group, which was rescued by CR and RALP treatment, especially the combination of CR and RALP (**Figure 9A**). We further assessed the effects of CR and RALP on the expression of overlapping targets in bone marrow. As illustrated in **Figure 9B**, both CR and RALP monotherapies effectively reduced the protein levels of CALM1, CHEK1, and MYC in the bone marrow. CR, but not RALP, uniquely upregulated ESR1 protein levels. Moreover, the combination treatment synergistically enhanced the reduction of CALM1 and the upregulation of ESR1. These *in vivo* results demonstrate that CR and RALP alleviate AML tumor burden, with the combination regimen showing superior efficacy.

Discussion

Our study demonstrates that CR and RALP individually inhibit proliferation and induce apoptosis in AML cells *in vitro*. *In vivo*, both

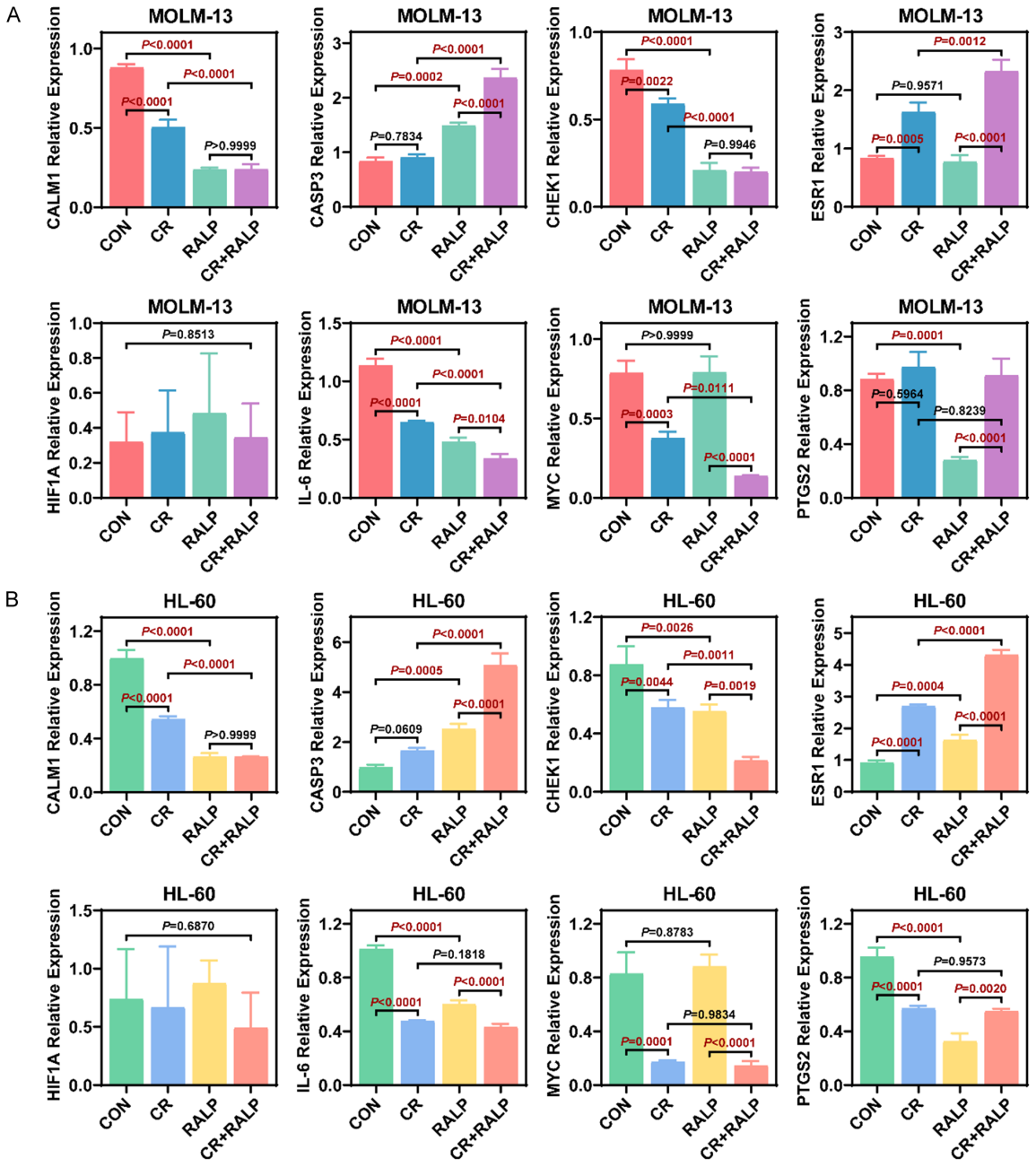

Figure 6. RALP and/or CR modulate target expression in MOLM-12 and HL-60 cells at mRNA level. (A, B) RT-qPCR was used to detect the mRNA levels of the overlapping targets (CALM1, CASP3, CHEK1, ESR1, HIF1A, IL-6, MYC, and PTGS2) in MOLM-12 (A) and HL-60 (B) cells from the Con, CR, RALP, and CR + RALP groups (n=3). RALP, Radix Aconiti Lateralis Preparata; CR, Coptidis Rhizoma; AML, acute myelocytic leukemia.

TCMs alleviated tissue or organ infiltration of Luc-MOLM-13 cells and decreased bone marrow hCD45$^+$ cells. Notably, CR and RALP acted synergistically to alleviate the overall AML tumor burden. These findings position CR and RALP as promising therapeutic agents for AML. The therapeutic action of many TCMs is mediated through multiple active ingredients acting on multiple targets. To investigate their mechanisms of action, we identified their active ingredients and AML-associated targets using network pharmacology. Key active ingredients identified in CR were berberine, obacunone, berberrubine, epiberberine, quercetin, copti-

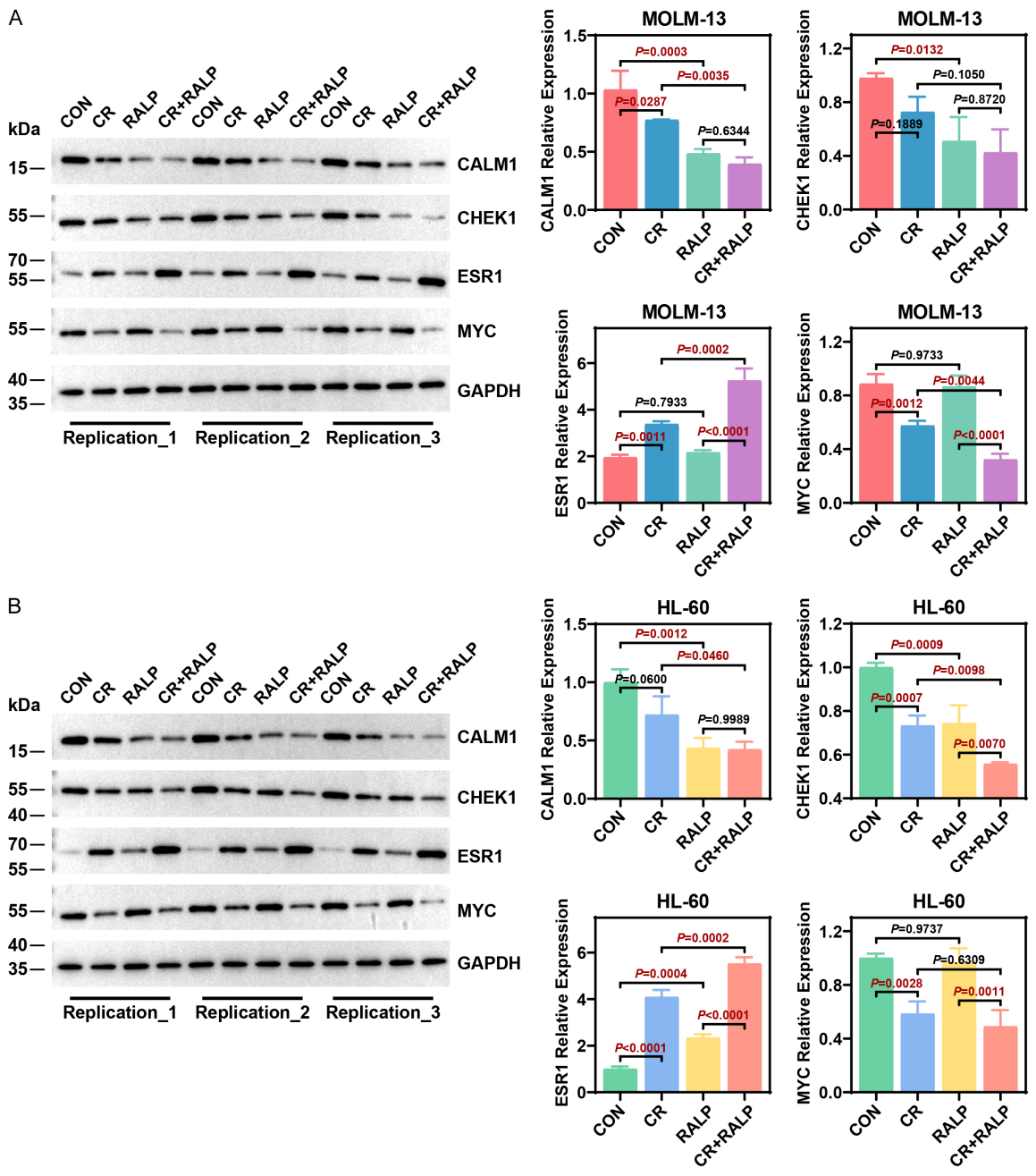

Figure 7. RALP and/or CR modulate target expression in MOLM-12 and HL-60 Cells at protein level. (A, B) Representative gel blot images and statistical analysis results of the overlapping targets (CALM1, CHEK1, ESR1, and MYC) in MOLM-12 (A) and HL-60 (B) cells from the Con, CR, RALP, and CR + RALP groups (n=3). RALP, Radix Aconiti Lateralis Preparata; CR, Coptidis Rhizoma; AML, acute myelocytic leukemia.

sine. In RALP, key ingredients included deoxyandrographolide, (R)-Norcoclaurine, sitosterol, delphin, deltoin. Notably, previous studies have demonstrated that berberine [26], obacunone [27], epiberberine [28], quercetin [29], coptisine [30], deoxyandrographolide [31], (R)-Norcoclaurine [32], and sitosterol [33] possess antileukemic effects by alleviating malignant phenotypes. This supports the premise that the anti-AML effects of CR and RALP is attributable, at least in part, to these active ingredients. To further elucidate the molecular mechanisms, we identified targets of these ingredients that are associated with AML pathogenesis. Our analysis pinpointed several potential key targets, including CASP3, CHEK1, ESR1,

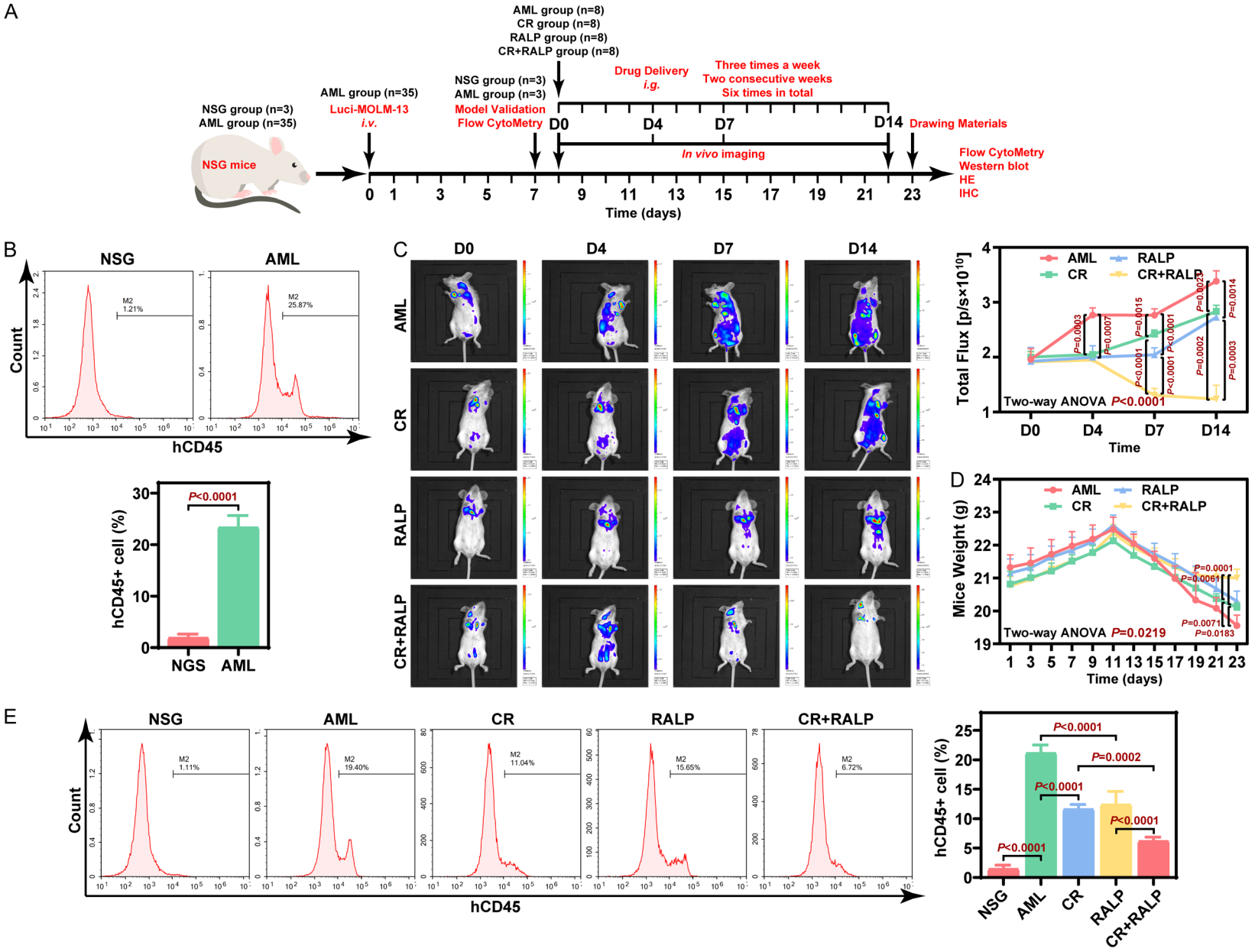
A
AML group (n=8)
CR group (n=8)
RALP group (n=8)
CR+RALP group (n=8)
NSG group (n=3)
AML group (n=35)
NSG group (n=3)
AML group (n=35)
Luci-MOLM-13
i.v.
NSG group (n=3)
AML group (n=3)
Model Validation
Flow CytoMetry
Drug Delivery
i.g.
Three times a week
Two consecutive weeks
Six times in total
D0
D4
D7
D14
Drawing Materials
In vivo imaging
NSG mice
Flow CytoMetry
Western blot
HE
IHC
0 1 3 5 7 9 11 13 15 17 19 21 23
Time (days)
B
NSG
AML
M2
1.21%
M2
25.87%
Count
hCD45
hCD45+ cell (%)
P<0.0001
NGS
AML
C
D0
D4
D7
D14
AML
CR
RALP
CR+RALP
Total Flux [p/s×10^10]
AML
RALP
CR
CR+RALP
P=0.0003
P=0.0007
P=0.0015
P=0.0001
P<0.0001
P<0.0001
P=0.0001
P=0.0002
P=0.0023
P=0.0014
P=0.0003
Two-way ANOVA P<0.0001
D0
D4
D7
D14
Time
D
Mice Weight (g)
AML
RALP
CR
CR+RALP
P=0.0001
P=0.0061
P=0.0071
P=0.0183
Two-way ANOVA P=0.0219
1 3 5 7 9 11 13 15 17 19 21 23
Time (days)
E
NSG
AML
CR
RALP
CR+RALP
M2
1.11%
M2
19.40%
M2
11.04%
M2
15.65%
M2
6.72%
Count
hCD45
hCD45+ cell (%)
P<0.0001
P=0.0002
P<0.0001
P<0.0001
P<0.0001
NSG
AML
CR
RALP
CR+RALP

Figure 8. RALP and/or CR mitigate the burden of AML *in vivo*. A. Flowchart of the development of the AML model and the timeline for CR and RALP administration in this study. B. On day 7 after Luc-MOLM-13 injection, flow cytometry was used to identify the content of hCD45$^+$ cells in the bone marrow of NSG and AML group mice (n=3). C. Representative images of *in vivo* imaging of NSG mice in the AML, CR, RALP, and CR+RALP groups and the differences in total flux at various time points (Days 0, 4, 7, and 14) (n=4). D. The effects of CR and/or RALP treatment on the weight of NSG mice with the relevant AML model (n=8). E. On day 23 post Luc-MOLM-13 injection, flow cytometry identified the differences in the proportion of hCD45+ cells in the bone marrow of NSG, AML, CR, RALP, and CR + RALP group mice (n=4). RALP, Radix Aconiti Lateralis Preparata; CR, Coptidis Rhizoma; AML, acute myelocytic leukemia.

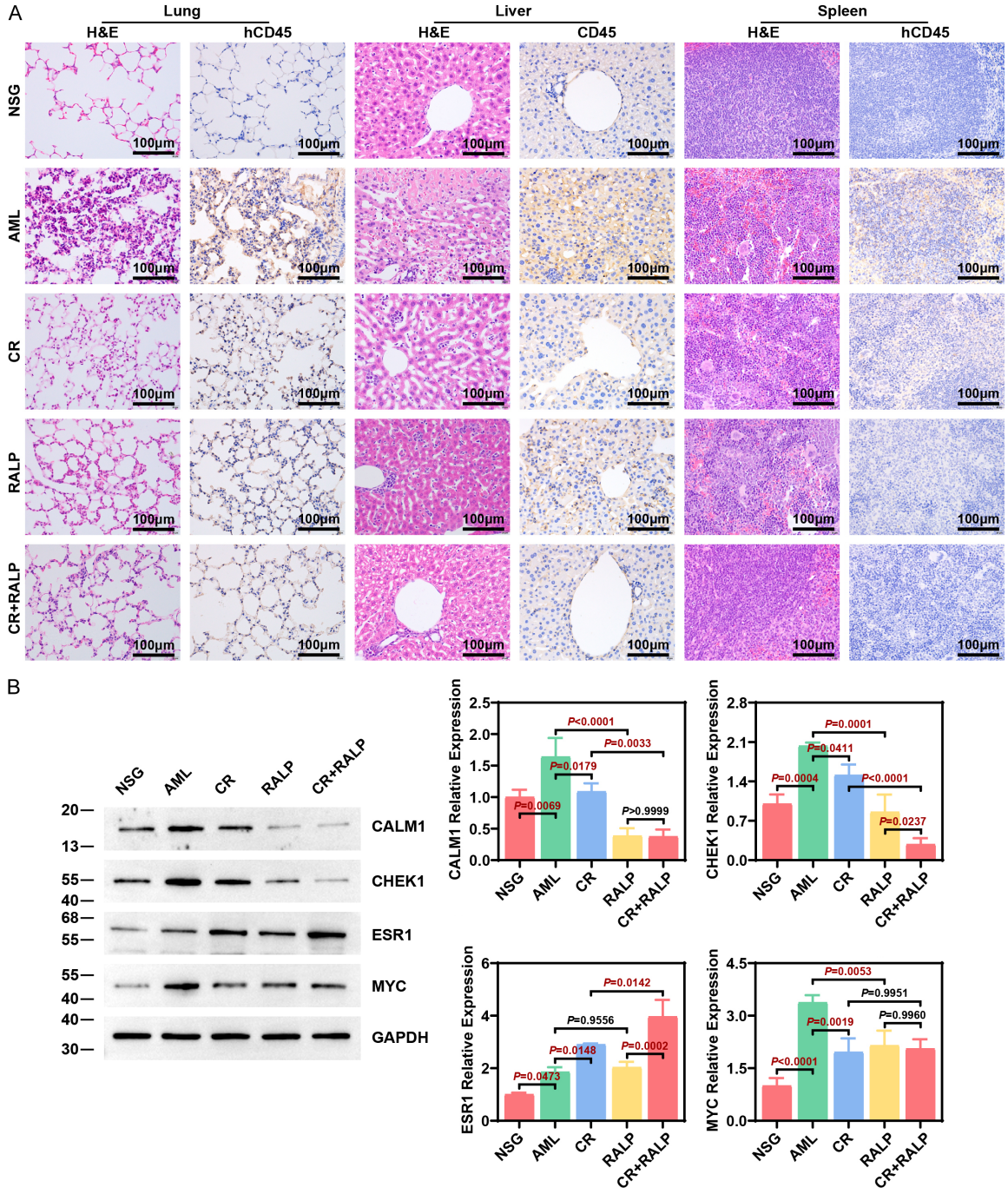

Figure 9. Effect of RALP and/or CR on organ lesions and expression of overlapping targets in AML *in vivo*. A. Representative images of hematoxylin-eosin staining and immunohistochemistry (hCD45) staining of the lungs, liver, and

spleen from NSG, AML, CR, RALP, and CR+RALP group mice (n=4). Scale = 100 μm. B. Western blot assay identified the expression differences of the overlapping targets (CALM1, CHEK1, ESR1, and MYC) of RALP and CR in the bone marrow of NSG, AML, CR, RALP, and CR + RALP group mice (n=3). RALP, Radix Aconiti Lateralis Preparata; CR, Coptidis Rhizoma; AML, acute myelocytic leukemia.

IL-6, MYC, PTGS2, and CALM1, which may be key targets for CR and RALP.

CASP3 is a central executioner caspase in apoptosis, integrating signals from both the exogenous (death receptor) and endogenous (mitochondrial) pathways. Upon activation, CASP3 cleaves numerous intracellular substrates, leading to the degradation of DNA, cytoskeletal components, and signaling molecules to execute apoptosis [34, 35]. We found that CR and RALP increased CASP3 expression in AML cells and in bone marrow of AML animal models. Thus, the upregulation of CASP3 represents one mechanism through which CR and RALP exert their anti-AML effects. CHEK1 is a key protein kinase regulating cell cycle checkpoints and DNA damage response. In AML, CHEK1 activity accelerates cell cycle and maintains genomic stability [36-39]. Additionally, CHEK1 inhibitors such as prexasertib, V158411, GDC0575, and CCT-245737 are under investigation as potential AML therapies [36-39]. Our finding that CR and RALP reduce CHEK1 expression in AML provides a plausible explanation for their antiproliferative activity in AML. MYC is a master regulator of tumor malignancy. Its overexpression or constitutive activation drives proliferation, metabolic reprogramming, evasion of apoptosis, angiogenesis, and metastasis in diverse cancers [40, 41]. In this study, both CR and RALP suppressed MYC expression. PTGS2, also known as COX-2, is a key synthase that catalyzes the conversion of arachidonic acid to prostaglandins, regulating physiological processes such as inflammation, pain, immunity [42, 43]. It is frequently overexpressed in a variety of tumors, including AML. We observed that CR and RALP attenuated PTGS2 levels in AML cells. Collectively, this evidence aligns with and elucidates the potential molecular mechanisms of CR and RALP against AML, underscoring their multi-target, multi-ingredient mode of action.

This study has several limitations that warrant consideration. CR and RALP are known to exert immunomodulatory effects in tumors [44, 45]. In our experimental design, a control group of healthy mice that received only CR and RALP treatment was not set up. Moreover, we did not conduct systematic monitoring of organ toxicity indicators during the treatment process, such as liver and kidney function and routine blood tests. Therefore, we were unable to systematically assess the potential toxicity or impact of RALP and CR on the normal hematopoietic system and organ tissues. Future research still needs to establish healthy drug controls to comprehensively evaluate its safety and therapeutic window, providing more sufficient experimental evidence for its clinical transformation. In AML, alterations in the tumor immune microenvironment compromise immune surveillance and facilitate tumor immune escape [46, 47]. This immune dysfunction severely undermines the efficacy of immunotherapies, including hematopoietic stem cell transplantation, CAR-T therapy, vaccine therapy, and immune checkpoint inhibitors [46, 47]. Consequently, CR and RALP represent promising candidates as immunomodulators or adjuvants for AML immunotherapy. Their specific roles in modulating AML immunity warrant further investigation. In conclusion, our findings demonstrate that CR and RALP alleviated AML tumor burden and exhibit synergistic activity. These results provide a foundation for developing CR and RALP as potential therapeutic agents or adjuvants for AML.

Acknowledgements

This study was supported by the National Natural Science Foundation of China (82260871), the Professor Hu Yu's Workstation of Yunnan Province (202305AF150149), the Yunnan Provincial Science and Technology Department (202101AC070530), and the Yunnan Provincial Science and Technology Department (202403AC100017).

Disclosure of conflict of interest

None.

Address correspondence to: Tong-Hua Yang and Peng Hu, Department of Hematology, The Affiliated Hospital of Kunming University of Science and Technology, No. 157 Jinbi Road, Kunming 650500, Yunnan, P. R. China. E-mail: 9y140214@kust.edu.cn; ynanblood@aliyun.com (THY); 20171136007@stu.kust.edu.cn; hupengkkxx@126.com (PH)

References

[1] Kayser S and Levis MJ. The clinical impact of the molecular landscape of acute myeloid leukemia. Haematologica 2023; 108: 308-320.

[2] Bray F, Laversanne M, Sung H, Ferlay J, Siegel RL, Soerjomataram I and Jemal A. Global cancer statistics 2022: GLOBOCAN estimates of incidence and mortality worldwide for 36 cancers in 185 countries. CA Cancer J Clin 2024; 74: 229-263.

[3] Forsberg M and Konopleva M. AML treatment: conventional chemotherapy and emerging novel agents. Trends Pharmacol Sci 2024; 45: 430-448.

[4] Strickland SA and Vey N. Diagnosis and treatment of therapy-related acute myeloid leukemia. Crit Rev Oncol Hematol 2022; 171: 103607.

[5] Senapati J, Kadia TM and Ravandi F. Maintenance therapy in acute myeloid leukemia: advances and controversies. Haematologica 2023; 108: 2289-2304.

[6] Gao X, Zuo X, Min T, Wan Y, He Y and Jiang B. Traditional Chinese medicine for acute myelocytic leukemia therapy: exploiting epigenetic targets. Front Pharmacol 2024; 15: 1388903.

[7] Zhong LL, Zheng Y, Lau AY, Wong N, Yao L, Wu X, Shao T, Lu Z, Li H, Yuen CS, Guo J, Lo S, Chau J, Chan KW, Ng BFL, Bian Z and Yu EC. Would integrated Western and traditional Chinese medicine have more benefits for stroke rehabilitation? A systematic review and meta-analysis. Stroke Vasc Neurol 2022; 7: 77-85.

[8] Cui H, Han S, Dai Y, Xie W, Zheng R, Sun Y, Xia X, Deng X, Cao Y, Zhang M and Shang H. Gut microbiota and integrative traditional Chinese and western medicine in prevention and treatment of heart failure. Phytomedicine 2023; 117: 154885.

[9] Jiang F, Xu N, Zhou Y, Song J, Liu J, Zhu H, Jiang J, Xu Y and Li R. Contribution of traditional Chinese medicine combined with conventional western medicine treatment for the novel coronavirus disease (COVID-19), current evidence with systematic review and meta-analysis. Phytother Res 2021; 35: 5992-6009.

[10] Yang M, Ji X and Zuo Z. Relationships between the toxicities of Radix Aconiti Lateralis Preparata (Fuzi) and the toxicokinetics of its main diester-diterpenoid alkaloids. Toxins (Basel) 2018; 10: 391.

[11] Wang J, Wang L, Lou GH, Zeng HR, Hu J, Huang QW, Peng W and Yang XB. Coptidis Rhizoma: a comprehensive review of its traditional uses, botany, phytochemistry, pharmacology and toxicology. Pharm Biol 2019; 57: 193-225.

[12] Zhang W, Ding M, Feng Y, Cai S, Luo Z, Shan J and Di L. Modulation of cellular metabolism and alleviation of bacterial dysbiosis by Aconiti Lateralis Radix Praeparata in non-small cell lung cancer treatment. Phytomedicine 2024; 126: 155099.

[13] Zhou X, Liu B, Ning Q, Xia Z, Zhong R, Zhang L and Wu L. Combination of Huanglian Jiedu Decoction and erlotinib delays growth and improves sensitivity of EGFR-mutated NSCLC cells in vitro and in vivo via STAT3/Bcl-2 signaling. Oncol Rep 2021; 45: 217-229.

[14] Hu Q, Liu Y, Yu J, Yang X, Yang M, He Y, Han L and Zhang D. The protective effect and antitumor activity of Aconiti Lateralis Radix Praeparata (Fuzi) polysaccharide on cyclophosphamide-induced immunosuppression in H22 tumor-bearing mice. Front Pharmacol 2023; 14: 1151092.

[15] Li M, Shang H, Wang T, Yang SQ and Li L. Huanglian decoction suppresses the growth of hepatocellular carcinoma cells by reducing CCNB1 expression. World J Gastroenterol 2021; 27: 939-958.

[16] Xu Y, Wang H, Wang T, Chen C, Sun R, Yao W, Ma Y, Zhang Q, Wu L, Zeng S and Sun X. Dahuang Fuzi Baijiang decoction restricts progenitor to terminally exhausted T cell differentiation in colorectal cancer. Cancer Sci 2022; 113: 1739-1751.

[17] Li XK, Motwani M, Tong W, Bornmann W and Schwartz GK. Huanglian, a Chinese herbal extract, inhibits cell growth by suppressing the expression of cyclin B1 and inhibiting CDC2 kinase activity in human cancer cells. Mol Pharmacol 2000; 58: 1287-1293.

[18] Kang JX, Liu J, Wang J, He C and Li FP. The extract of huanglian, a medicinal herb, induces cell growth arrest and apoptosis by upregulation of interferon-beta and TNF-alpha in human breast cancer cells. Carcinogenesis 2005; 26: 1934-1939.

[19] Ru J, Li P, Wang J, Zhou W, Li B, Huang C, Li P, Guo Z, Tao W, Yang Y, Xu X, Li Y, Wang Y and Yang L. TCMSP: a database of systems pharmacology for drug discovery from herbal medicines. J Cheminform 2014; 6: 13.

[20] Piñero J, Saüch J, Sanz F and Furlong LI. The DisGeNET cytoscape app: exploring and visualizing disease genomics data. Comput Struct Biotechnol J 2021; 19: 2960-2967.

[21] Szklarczyk D, Gable AL, Lyon D, Junge A, Wyder S, Huerta-Cepas J, Simonovic M, Doncheva NT, Morris JH, Bork P, Jensen LJ and Mering CV. STRING v11: protein-protein association networks with increased coverage, supporting functional discovery in genome-wide experimental datasets. Nucleic Acids Res 2019; 47: D607-D613.
[22] Wu T, Hu E, Xu S, Chen M, Guo P, Dai Z, Feng T, Zhou L, Tang W, Zhan L, Fu X, Liu S, Bo X and Yu G. clusterProfiler 4.0: a universal enrichment tool for interpreting omics data. Innovation (Camb) 2021; 2: 100141.
[23] Ginestet C. ggplot2: elegant graphics for data analysis. Journal of the Royal Statistical Society Series A: Statistics in Society 2011; 174: 245-246.
[24] Zhang S, Feng R, Bai J, Ning S, Xu X, Sun J, Wu M and Liu H. CDK7 inhibition induces apoptosis in acute myeloid leukemia cells and exerts synergistic antileukemic effects with azacitidine in vitro and in vivo. Leuk Lymphoma 2023; 64: 639-650.
[25] Wu G, Guo S, Luo Q, Wang X, Deng W, Ouyang G, Pu JJ, Lei W and Qian W. Preclinical evaluation of CD70-specific CAR T cells targeting acute myeloid leukemia. Front Immunol 2023; 14: 1093750.
[26] Huang Z, Shen Y, Liu W, Yang Y, Guo L, Yan Q, Wei C, Guo Q, Fan X and Ma W. Berberine targets the electron transport chain complex I and reveals the landscape of OXPHOS dependency in acute myeloid leukemia with IDH1 mutation. Chin J Nat Med 2023; 21: 136-145.
[27] Jung H, Sok DE, Kim Y, Min B, Lee J and Bae K. Potentiating effect of obacunone from Dictamnus dasycarpus on cytotoxicity of microtuble inhibitors, vincristine, vinblastine and taxol. Planta Med 2000; 66: 74-76.
[28] Li ZR, Suo FZ, Guo YJ, Cheng HF, Niu SH, Shen DD, Zhao LJ, Liu ZZ, Maa M, Yu B, Zheng YC and Liu HM. Natural protoberberine alkaloids, identified as potent selective LSD1 inhibitors, induce AML cell differentiation. Bioorg Chem 2020; 97: 103648.
[29] Torello CO, Alvarez MC and Olalla Saad ST. Polyphenolic flavonoid compound quercetin effects in the treatment of acute myeloid leukemia and myelodysplastic syndromes. Molecules 2021; 26: 5781.
[30] Lin CC, Ng LT, Hsu FF, Shieh DE and Chiang LC. Cytotoxic effects of Coptis chinensis and Epimedium sagittatum extracts and their major constituents (berberine, coptisine and icariin) on hepatoma and leukaemia cell growth. Clin Exp Pharmacol Physiol 2004; 31: 65-69.
[31] Chen L, Zhu H, Wang R, Zhou K, Jing Y and Qiu F. ent-Labdane diterpenoid lactone stereoisomers from Andrographis paniculata. J Nat Prod 2008; 71: 852-855.
[32] Yang C, Fang Y, Hu Y, Tian T and Liao G. Discovery of new tetrahydroisoquinolines as potent and selective LSD1 inhibitors for the treatment of MLL-rearranged leukemia. Eur J Med Chem 2023; 257: 115516.
[33] Wang H, Wang Z, Zhang Z, Liu J and Hong L. β-Sitosterol as a promising anticancer agent for chemoprevention and chemotherapy: mechanisms of action and future prospects. Adv Nutr 2023; 14: 1085-1110.
[34] Asadi M, Taghizadeh S, Kaviani E, Vakili O, Taheri-Anganeh M, Tahamtan M and Savardashtaki A. Caspase-3: structure, function, and biotechnological aspects. Biotechnol Appl Biochem 2022; 69: 1633-1645.
[35] Eskandari E and Eaves CJ. Paradoxical roles of caspase-3 in regulating cell survival, proliferation, and tumorigenesis. J Cell Biol 2022; 221: e202201159.
[36] Bryant C, Scriven K and Massey AJ. Inhibition of the checkpoint kinase Chk1 induces DNA damage and cell death in human Leukemia and Lymphoma cells. Mol Cancer 2014; 13: 147.
[37] Ostergaard J, Jonart LM, Ebadi M, Koppenhafer SL, Gordon DJ and Gordon PM. Preclinical efficacy of prexasertib in acute lymphoblastic leukemia. Br J Haematol 2021; 194: 1094-1098.
[38] Di Tullio A, Rouault-Pierre K, Abarrategi A, Mian S, Grey W, Gribben J, Stewart A, Blackwood E and Bonnet D. The combination of CHK1 inhibitor with G-CSF overrides cytarabine resistance in human acute myeloid leukemia. Nat Commun 2017; 8: 1679.
[39] Fan Z, Luo H, Zhou J, Wang F, Zhang W, Wang J, Li S, Lai Q, Xu Y, Wang G, Liang A and Xu J. Checkpoint kinase-1 inhibition and etoposide exhibit a strong synergistic anticancer effect on chronic myeloid leukemia cell line K562 by impairing homologous recombination DNA damage repair. Oncol Rep 2020; 44: 2152-2164.
[40] Llombart V and Mansour MR. Therapeutic targeting of "undruggable" MYC. EBioMedicine 2022; 75: 103756.
[41] Das SK, Lewis BA and Levens D. MYC: a complex problem. Trends Cell Biol 2023; 33: 235-246.
[42] Kaur B and Singh P. Inflammation: biochemistry, cellular targets, anti-inflammatory agents and challenges with special emphasis on cyclooxygenase-2. Bioorg Chem 2022; 121: 105663.
[43] Kulesza A, Paczek L and Burdzinska A. The role of COX-2 and PGE2 in the regulation of immunomodulation and other functions of mesenchymal stromal cells. Biomedicines 2023; 11: 445.

[44] Zhang W, Lu C, Cai S, Feng Y, Shan J and Di L. Aconiti Lateralis Radix Praeparata as potential anticancer herb: bioactive compounds and molecular mechanisms. Front Pharmacol 2022; 13: 870282.
[45] Kim E, Ahn S, Rhee HI and Lee DC. Coptis chinensis Franch. Extract up-regulate type I helper T-cell cytokine through MAPK activation in MOLT-4 T cell. J Ethnopharmacol 2016; 189: 126-131.
[46] Vago L and Gojo I. Immune escape and immunotherapy of acute myeloid leukemia. J Clin Invest 2020; 130: 1552-1564.
[47] Tettamanti S, Pievani A, Biondi A, Dotti G and Serafini M. Catch me if you can: how AML and its niche escape immunotherapy. Leukemia 2022; 36: 13-22.